Influence of Graft Density on Kinetics of Surface-Initiated ATRP of Polystyrene from Montmorillonite

Ross E. Behling, Bryce A. Williams, Brandy L. Staade, Lynn M. Wolf, and Eric W. Cochran*

Department of Chemical and Biological Engineering, Iowa State University, Ames, Iowa 50010

Received November 6, 2008; Revised Manuscript Received February 3, 2009

ABSTRACT: Here we report the kinetics of the surface-initiated atom transfer radical polymerization (ATRP) of styrene from the surface of functionalized montmorillonite clay as a function of graft density. Compared with analogous ATRP reactions with free initiator, we observe a seven-fold increase in the polymerization rate at the highest graft density, ∼1 chain/nm^2, whereas bulk kinetics are recovered as the graft density is reduced. We hypothesize that this phenomenon is a consequence of local concentration heterogeneities that shift the ATRP equilibrium in favor of the active state and present a simple phenomenological kinetic model that accounts for our data. These findings present an important consideration relevant to the design of precisely defined molecular architectures from surfaces via surface-initiated ATRP.

1. Introduction

Atom transfer radical polymerization (ATRP) has proven to be a versatile method for synthesizing polymers of narrow polydispersity at targeted molecular weights.[1] ATRP provides an industrially scalable process by means of an inexpensive copper-mediated halide exchange using commercially available ligands to facilitate catalyst solubility.[2,3] In more recent years, researchers have realized the potential for utilizing ATRP to modify the surface chemistry of many materials. Colloidal silica,[4] montmorillonite clay (MMT),[5] gold films,[6−8] and silicon wafers[9−11] have been the most frequently studied substrates for surface-initiated (SI)-ATRP, where the first is a spherical particle and the last three are high-aspect-ratio materials.

The study of polymer brushes advances many fields of science and technology through the production of stimuli-responsive interfaces,[12,13] the improvement of colloidal stability,[14] and the synthesis of nanocomposites.[15−17] Polymer brushes are used to alter physical properties such as surface wetting and roughness as well as to add chemical functionality. Stimuli-responsive materials have been shown to respond to temperature, pH, and solvent quality among other environmental factors. In principle, the physical and chemical properties of the brush layer may be precisely tuned through the monomer chemistry, polymer architecture, and molecular weight distribution, which in turn may be controlled only with a thorough understanding of the polymerization chemistry.

In the context of ATRP, the apparent polymerization rate, R_p, is governed by the equilibrium between dormant and active chains through reactions with the catalyst system. In SI-ATRP, the spatial proximity of the chain ends is significantly closer than in an analogous bulk polymerization, where the catalyst system is homogeneously distributed throughout the reaction media. These confinement effects can have a marked influence on R_p; to date, studies relating the kinetics of SI-ATRP to those in bulk media have thus far yielded conflicting and sometimes orthogonal conclusions.[4,7,8,10,18]

Substrate geometry and graft density should play key roles in the reaction kinetics of SI-ATRP. Densely grafted spherical particles, for instance, initially feature an average chain-end-to-chain-end distance that is drastically smaller than in an "analogous" bulk system containing the same number of chain ends per volume. One may reasonably speculate that surface-confinement effects should be significant in this scenario. However, as the brush thickness increases, propagating radicals should spatially diverge from one another and recover bulk kinetic rates because the distance between chain ends scales with the particle radius. Consistent with this notion, Fukada et al. studied the kinetics of an SI-ATRP from functionalized monodisperse silica particles ranging from 100 to 1500 nm in diameter with the inclusion of an unbound "sacrificial" initiator and found both species' kinetic rates to be equivalent.[4]

Whereas SI-ATRP from spherical particles evidently assumes bulk kinetics, SI polymerization from planar substrates should be expected to exhibit confinement effects irrespective of the brush thickness. Literature studies of polymer brushes have focused largely on gold and silicon substrates that may be viewed as infinite planes; additionally, MMT clays approximate this geometry owing to their high aspect ratio.

Unfortunately, the number of investigations that explicitly account for surface confinement effects is limited. Early reports in the field indicate that R_p decreases with time attributed to termination reactions that were not suppressed because of an inadequate supply of deactivating copper(II) ($Cu^{II}X_2$) species.[6,19] This may be understood by considering that only microscopic quantities of $Cu^{II}X_2$ are generated through the activation of dormant sites on the surface, which are then diluted into the macroscopic quantity of monomer/solvent in which the substrate is immersed. These termination effects may be circumvented through the introduction of excess $Cu^{II}X_2$ or unbound initiator at the onset of polymerization.[20]

There is some evidence of the living character of SI-ATRP reactions depending on the monomer; for example, a number of reports indicate linear monomer conversion versus time in poly(methyl methacrylate) (PMMA),[8,11] whereas R_p plateaus in polymerizations of poly(*N*-isopropylacrylamide),[7] polyacrylamide,[9] or poly(glycidyl methacrylate) (PGMA).[8]

The role of graft density, ρ_g, on R_p is unclear. Huck et al. investigated a series of PMMA brushes on gold substrates and found no dependence, although direct comparisons with bulk polymerization rates were not available.[8] Genzer et al. studied graft density effects using a gradient approach in poly(acrylamide) (PAA) and found that in the brush regime the thickness scaled as $\rho_g^{1/3}$, suggesting that all chains along the gradient were the same size.[10]

* To whom correspondence should be addressed. E-mail: ecochran@iastate.edu. Fax: (515) 294-2689.

10.1021/ma8024909 CCC: $40.75
Published on Web 02/27/2009

However, Fukuda et al. reported that the brush height in a PMMA system from silica wafers at moderate graft density obeyed the $\rho_g^{1/3}$ law, but at high graft density ($\rho_g > 0.7$ chains/nm^2) it approached $\rho_g^{1/2}$; again, direct molecular weight measurements of the brush layer were not conducted and so here the possibility of an R_p dependence on ρ_g cannot be discounted.[18]

In this article, we report a strong dependence of R_p on ρ_g in SI-ATRP of polystyrene (PS) from MMT. At high graft density, ~1 chain/nm^2, we have observed an apparent polymerization rate that is nearly an order of magnitude larger than that of the analogous bulk system, which rapidly decays to the bulk kinetics as ρ_g is reduced. We hypothesize that this phenomenon is a consequence of local concentration heterogeneities that shift the equilibrium in favor of the active state and present a simple phenomenological model that accounts for our data.

2. Experimental Details

Functionalization of Montmorillonite. MMT was generously supplied by Southern Clay Products (92 (mequiv)/(100 g)). On the basis of the ion exchange capacity and measurements of the specific surface area,[21] MMT contains ~1site/nm^2. MMT was functionalized via ion exchange with a combination of 11′(*N*,*N*,*N*-trimethylammonium bromide)-undecyl-2-bromo-2-methyl propionate (BMP) and 11′(*N*,*N*,*N*-trimethylammonium bromide)-undecyl-2,2-dimethyl propionate (DMP).

The synthesis and ion exchange of BMP, an ATRP initiator, with MMT is a simple two-step synthesis that was previously described elsewhere.[5,22] It may be summarized as the addition of 2-bromoisobutyryl bromide to 11-bromo-1-undecanol and the subsequent addition of trimethyl amine to produce a cationic alkyl chain with a terminal halide. The synthesis of an analogous inert compound, DMP, uses 2,2-dimethyl acetyl chloride in place of 2-bromoisobutyryl bromide. 2-Bromoisobutyryl bromide, ethyl-2-bromopropionate (EBP), and 2,2-dimethyl acetyl chloride were purchased from Aldrich Chemical and used as received. BMP and DMP can then be mixed into desired molar ratios and ion exchanged to produce specified active graft densities.

Atom Transfer Radical Polymerization of Styrene. Benzyl bromide (BBr), copper(II) bromide ($Cu^{II}Br_2$), *N*,*N*,*N*′,*N*″,*N*″- pentamethyldiethylenetriamine (PMDETA), and *tert*-butylacetyl chloride were purchased from Aldrich Chemical and used without further purification. Copper(I) bromide ($Cu^{I}Br$) was purchased from Aldrich Chemical and purified with acetic acid.[23] Styrene was purchased from Fisher Scientific, purified over basic alumina, and degassed prior to use. The unconfined ATRP of PS from either BBr or ethyl-2-methyl-2-bromopropionate (EBP) followed the procedure described in numerous articles by Matyjaszewski et al.[1−3] SI-ATRP of PS from MMT was similar to the work of others,[5,22] with the addition of ultrasonication to enhance MMT tactoid dispersion. Monomer, initiator, $Cu^{I}Br$, $Cu^{II}Br_2$, and PMDETA were mixed under N_2 in a round-bottomed flask with molar ratios of 1000:1:1:0.06:1.06, respectively. All polymerizations were conducted at 100 °C. Aliquots of PS brushes were cleaved from MMT over basic alumina for molecular weight analysis. Molecular weight distributions were determined by size exclusion chromatography (SEC).

3. Results

To control the polymer graft density systematically, a series of MMT compounds was prepared via complete ion exchange with mixtures consisting of a mole fraction, σ, of BMP (ATRP-active) and (1 − σ) DMP (dormant) surfactants, depicted schematically in Figure 1. Figure 2 demonstrates that this process occurs in a two-stage addition (the first after 48 h and the second by 96 h) and that longer mixing times do not further enhance XRD *d* spacing. Figure 3 displays all XRD *d* spacings and corresponding TGA data, which show that the fraction of volatiles reaches a maximum after 96 h of ion exchange.[24] Given the chemical similarity of BMP and DMP, we assert that the composition of the surface-bound ligands is essentially identical to that in the bulk medium, and thus the graft density of active initiators MMT-PS materials may be estimated to be $\rho_g = \sigma\rho_{g,max}$. The maximal graft density, $\rho_{g,max}$, is ~1 nm^{-2}, as calculated from the estimated specific surface area of MMT, 600 m^2/g,[21] and ion exchange capacity of 0.92 mequiv/g.

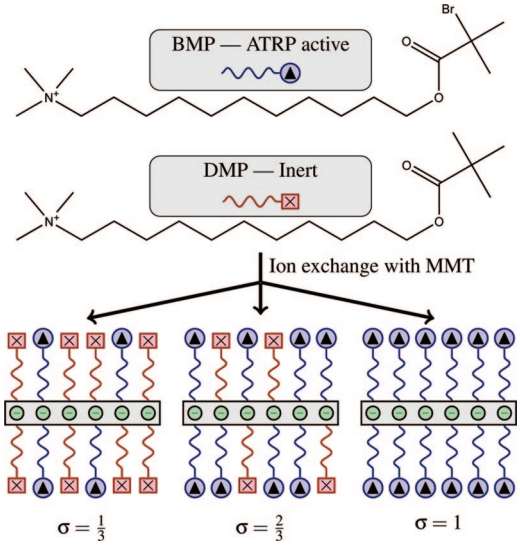

Figure 1. Route to MMT with precisely defined graft densities prepared via complete ion exchange with mixtures composed of a mole fraction, σ, of ATRP-active alkyl−ammonium surfactants.

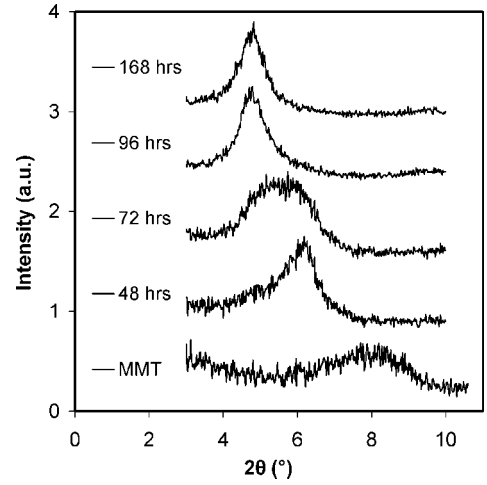

Figure 2. X-ray diffraction spectrum demonstrating the two-stage addition of initiator to MMT during ion exchange. As is evidenced by comparison of 96 and 168 h traces, no further ion exchange occurs after 96 h.

ATRP bulk reactions were conducted using unbound EBP or BBr as the initiator using molar ratios of monomer, initiator, $Cu^{I}Br$, $Cu^{II}Br_2$, and PMDETA equal to 1000:1:1:0.06:1.06. In reactions where molecular weights in excess of 100 kDa were expected, monomer-to-initiator molar ratios were increased to 1500:1 to maintain low polydispersity. Significant improvement in reproducibility was realized by premixing $Cu^{I}Br$ with $Cu^{II}Br_2$ in a 16:1 molar ratio prior to use. The addition of $Cu^{II}Br_2$ also served to slow propagation so that growth of chains within the interior of the clay galleries was not diffusion-limited.

A series of control experiments from unbound initiators employed either BBr or EBP as the initiator system. BBr was chosen for its chemical similarity to the monomer, whereas EBP was chosen to provide a closer comparison to the surface-tethered initiator species (BMP). Included in the control

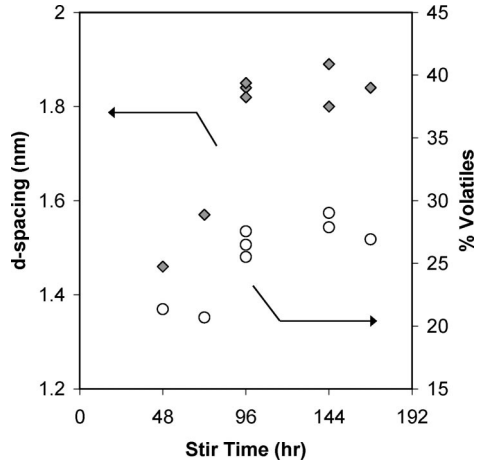

Figure 3. X-ray diffraction (◆) and thermogravimetric analysis (○) data demonstrating that by 96 h of stirring the maximum ion exchange has occurred.

Table 1. Results of ATRP Polymerization of Bulk and Confined Polystyrene Systems

initiator	time (h)	M_n (kDa)	PDI	$conv_{theor}$	$conv_{exptl}$	dM_n/dt (kDa/h)
BBr	6	23.3	1.11	0.224	NA	
BBr	12	35.8	1.12	0.345	NA	1.89
BBr	24	59.1	1.24	0.569	NA	
EBP	6	22.7	1.05	0.219	0.264	
EBP	12	43.4	1.07	0.416	0.131	1.89
EBP	24	56.4	1.07	0.542	0.542	
33%-MMT	6	21.5	1.20	0.069	0.071	
33%-MMT	12	35.6	1.15	0.114	0.101	2.54
33%-MMT	24	75.9	1.28	0.243	0.178	
67%-MMT	6	30.4	1.12	0.195	0.146	
67%-MMT	12	51.5	1.09	0.330	0.192	3.61
67%-MMT	24	101.5	1.16	0.520	0.479	
100%-MMT	3	64.5	1.11	0.620	NA	12.9
100%-MMT	6	96.4	1.12	0.927	NA	
10:1 100%-MMT/EBP	6	39.9/80.8	1.08/1.01	NA	NA	

experiments was a series of unbound initiator syntheses in the presence of pristine MMT; no discernible effect was measured via SEC as a result of the unfunctionalized MMT additive. The SEC results obtained for BBr and EBP were comparable in all experiments, although EBP exhibited a modest improvement in overall PDI. The decrease in PDI can be attributed to the faster initiation of the EBP species, resulting in a more uniform initiation of polymer chains. A representative sample of bulk and confined SEC results are shown in Table 1.

To assess the initiator efficiency of the MMT-initiated polymerizations, we compared the monomer conversion as measured by total yield with the theoretical conversion calculated from M_n assuming 100% initiator activity. From these data, we conclude that we reproducibly achieve at least 95% initiator efficiency in all systems.

Figure 4 compares the rates of polymerization for bulk PS and MMT-PS with three different graft densities, with the MMT samples listed in order of the mole percent active initiator (BMP). Immediately evident from inspection of Figure 4 is that R_p for PS grafted from 100%-MMT is nearly an order of magnitude greater than unbound PS produced under analogous conditions. The SI-ATRPs of styrene from 33%-MMT and 67%-MMT are also accelerated relative to bulk kinetics but lie between bulk and 100%-MMT values, respectively. Clearly, MMT graft density has a profound influence on the apparent propagation rate. The nonzero intercepts of the kinetic data appearing in Figure 4 are also noteworthy and likely indicate a short induction period during which uncontrolled polymerization

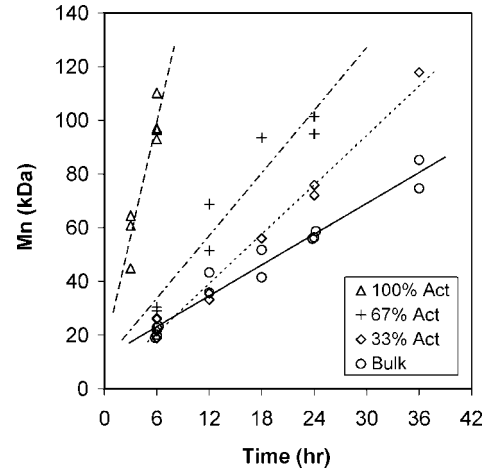

Figure 4. Bulk and confined polystyrene kinetic rates with active initiator percentages shown as 100%-MMT (△), 67%-MMT (+), 33%-MMT (◇), and bulk (○). Samples are shown with a linear fit to guide the eye.

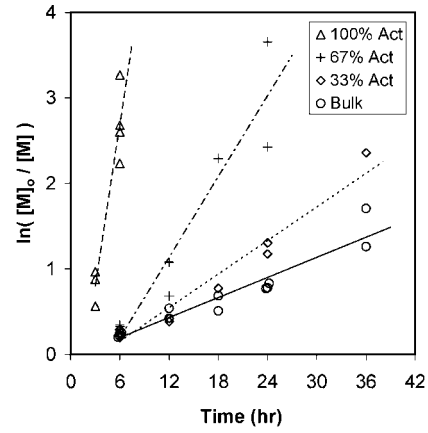

Figure 5. Bulk and confined polystyrene kinetic rates with active initiator percentages shown as 100%-MMT (△), 67%-MMT (+), 33%-MMT (◇), and bulk (○). Samples are shown with a linear fit to guide the eye.

proceeded prior to the development of the persistent radical effect.

All polymerizations exhibited living character with linear monomer consumption versus time for all graft densities (Figure 5). Successful reinitiation of MMT-PS brushes gave further evidence of termination reactions being effectively suppressed. To avoid clay aggregation, sufficient solvent needed to be present in the system to disperse MMT platelets. Therefore, in our system where monomer was used in excess as a solvent, we maintained a constant reaction volume by preparing molar ratios of monomer to combined active and inactive initiator concentrations. The resulting monomer to active initiator molar ratios were bulk 1000:1, 100%-MMT 1000:1, 67%-MMT 1500:1, and 33%-MMT 3000:1. Figure 6 clearly illustrates the expected differences in M_n versus conversion, and results agree with theoretical conversion limits for all graft densities. Figure 6 also presents the PDIs for all graft densities, demonstrating good molecular weight control up to 80% conversion; a loss of PDI control of ATRP reactions at high conversions is well documented in the literature.

To assess the potential influence of the MMT particle itself on the polymerization kinetics, we conducted experiments using a mixture of tethered 100%-MMT initiator and free EBP. A representative SEC trace appears in Figure 7, which shows the results from a polymerization using a 10:1 molar ratio of 100%-

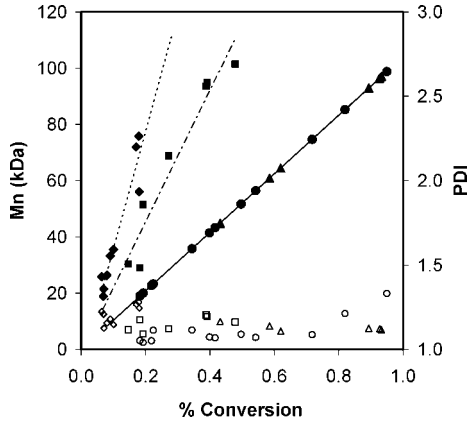

Figure 6. Bulk and confined polystyrene kinetic rates with active initiator percentages shown as 100%-MMT (△), 67%-MMT (□), 33%-MMT (◇), and bulk (○). Open and closed symbols correspond to PDI and M_n, respectively. Samples are shown with a linear fit to guide the eye.

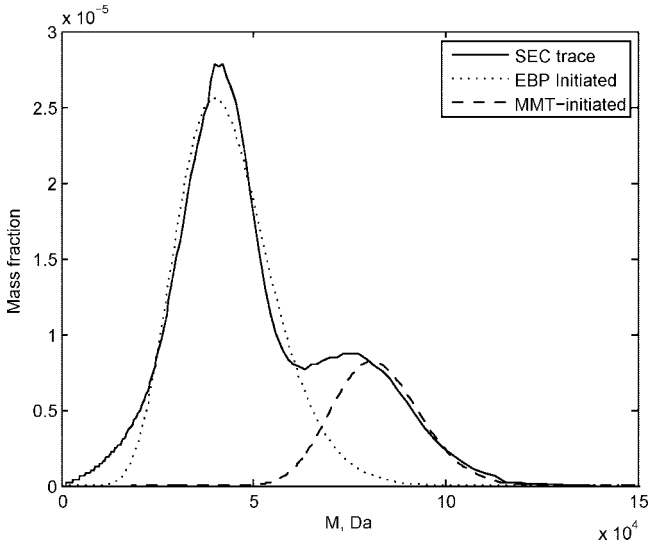

Figure 7. Representative SEC trace showing the molecular weight distribution from an ATRP at 100 °C initiated from a 10:1 molar ratio of 100%-MMT and EBP.

MMT/EBP at 100 °C for 6 h. The distribution is bimodal and was deconvolved via least-squares regression to a bimodal Schulz−Zimm distribution yielding $M_{n,MMT} = 80.8$ kDa and $M_{n,EBP} = 39.9$ kDa. The mass fraction of the MMT distribution in the SEC sample is evidently ∼23%, which reflects the repartitioning of the free versus tethered chains during the removal of grafted chains in the sample preparation.

To assess the degree of exfoliation of the MMT-PS materials, representative samples were sectioned using a diamond knife at cryogenic temperatures (−100 °C) with a Leica UCT ultramicratome. Light diffraction indicated an average section thickness of ∼100 nm. Polymer sections were transferred to copper grids and exposed to RuO_4 vapor. MMT makes an excellent barrier to RuO_4 deposition, resulting in strong contrast of MMT sheets. As can be seen in Figure 8, discrete MMT platelets are easily visible and display complete exfoliation.

4. Discussion

In conventional uncontrolled free radical polymerization, autoacceleration is frequently observed at high molecular weight because of viscosity effects, that is, the Trommsdorff effect. The Trommsdorff effect attributes faster kinetics at high conversion because of the elevated viscosity, which disproportionately hinders termination reactions by limiting the mobility of large molecules, favoring propagation. Here we believe that kinetic enhancement occurs not because of a reduction in termination reactions, which are already strongly suppressed in ATRP, but rather because of local concentration heterogeneities that shift the equilibrium, governing how frequently a chain is in its active state. The essence of our argument lies in the fact that all of the active sites (chain ends) in this surface-initiated system are constrained to reside in a volume that is significantly smaller than the macroscopic reaction volume. The consequences of this, directly related to the graft density, are twofold: (1) The local viscosity in the vicinity of reactive front will be significantly elevated compared with the macroscopic average. (2) The rms separation between active sites will be dramatically lower than that in a corresponding homogeneous ATRP. We assert that the result of these considerations is that within the growing viscous front, there is a repartitioning of the activating and deactivating catalyst species that directly leads to an elevation of the probability that any given chain end will be in its active state.

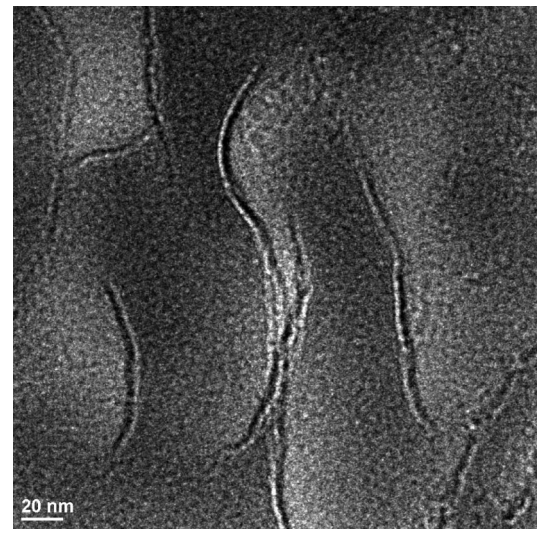

Figure 8. Electron micrograph of single montmorillonite silicate particles with grafted polystyrene chains shown to be very well exfoliated. Contrast results from RuO_4 deposition, where clay particles pose an excellent permeation barrier.

ATRP suppresses termination reactions via the so-called "persistent radical effect", an equilibrium between dormant polymer chains and propagating free radicals, where the dormant state is typically favored by many orders of magnitude depending on ligand quality

$$\mathrm{PX} + \mathrm{Cu^{I}X} \overset{K}{\rightleftharpoons} \mathrm{P^{\bullet}} + \mathrm{Cu^{II}X_2} \tag{1}$$

$$\mathrm{P^{\bullet}}_i + [\mathrm{M}] \xrightarrow{k_p} \mathrm{P^{\bullet}}_{i+1} \tag{2}$$

It is useful at this point to consider a kinetic model in terms of how fast, on average, a single chain is growing. This is simply the total polymerization rate times the monomer molecular mass, M_0, divided by the total number of chains in the system per volume, which can be approximated to be [PX]. Equation 3 defines the rate of polymerization of each chain in terms of the rate constant of propagation k_p, monomer concentration [M], and the probability that any chain is in its active state [P•]/[PX]

$$\frac{\mathrm{d}M_n}{\mathrm{d}t} = \frac{M_0 R_p}{[\mathrm{PX}]} = k_p[\mathrm{M}]\frac{[\mathrm{P^{\bullet}}]}{[\mathrm{PX}]} \tag{3}$$

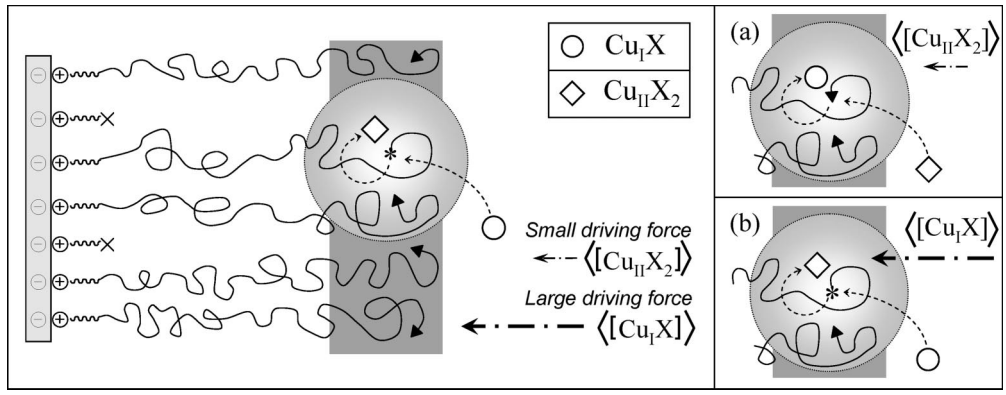

Figure 9. Schematic of the surface-initiated ATRP of polymer from MMT with the dark-gray box portraying the "growing viscous front" of small but finite thickness. Legend: Halide terminated chains (▲), nonfunctional initiators (×), and an active chain (*). In this region, there is a locally elevated concentration of chain ends, which observe local concentration heterogeneities resulting from the conversion of (a) Cu^{II} (◊) to Cu^{I} (○) or (b) Cu^{I} to Cu^{II}. The bulk catalyst concentrations then work to re-establish equilibrium, where the more abundant Cu^{I} has a much stronger driving force and lower steric resistance to mass transfer.

In a truly pseudo-first-order system, such as anionic polymerization or even uncontrolled free radical polymerization, the local concentration of active centers would assume a constant value throughout the system, irrespective of any local concentration inhomogeneities. The activation probability [P•]/[PX] in ATRP is governed by the activation−deactivation equilibrium and may be expressed as

$$\frac{[P\bullet]}{[PX]} = K\frac{[Cu^{I}X]}{[Cu^{II}X_2]} \tag{4}$$

where K is the equilibrium constant between active and dormant chains and has previously been reported for styrene, using 4,4′-di-(5-nonyl)-2,2′-bipyridine as a ligand, to favor the dormant state by seven orders of magnitude.[25] This model for SI-ATRP equilibrium was similarly derived by Xiao and Wirth when studying SI-ATRP of acrylamide from silica.[9] In a bulk ATRP, the equilibrium value of $[Cu^{I}X]/[Cu^{II}X_2]$ is homogeneous throughout the system, and thus the pseudo-first-order character of the polymerization is preserved.

In the present system, however, all of the chain ends are confined within a "viscous front" of small but finite thickness, separated from the bulk media by a region enriched in polymer chains. The local density of initiation sites is zero except within this "growing viscous front", depicted schematically in Figure 9.

Within the "viscous front", the local concentration must be related to the mean interparticle spacing, which is a function of initiator density and scales as $(\sigma\rho_{g,max})^{-1/2}$. The average volume that may be assigned to each initiation site must then scale as $(\sigma\rho_{g,max})^{-3/2}$, and accordingly the local chain end concentration scales as $(\sigma\rho_{g,max})^{3/2}$.The diffusion of activating and deactivating catalyst through the viscous front will be suppressed because of its enrichment with viscous polymer. Now consider an isolated propagating chain within this region: any encounter with a $Cu^{II}X_2$ complex that results in a deactivation reaction will deplete the local environment of a single $Cu^{II}X_2$ while enriching it with $Cu^{I}X$ (Figure 9a). The action of diffusion will work rapidly to restore this local disruption to a homogeneous state. However, over sufficiently small time and length scales, there will be a finite elevation of $Cu^{I}X$ balanced by the depletion of $Cu^{II}X_2$. Concretely, at some position, **r**, and time, t, from its formation, the probability of finding an "extra" $Cu^{I}X$ scales as $t^{-3/2}e^{-r^2/t}$. In a similar vein, the dynamics of replenishment of $Cu^{II}X_2$ will be governed by its diffusion from the bulk media. For the activation/deactivation kinetics to be influenced, there must be other chain ends present at small enough values of $|r|$ for this probability to be nonvanishing. In Figure 9, the position dependence of the probability with $|\mathbf{r}|$ is illustrated with a color gradient centered around the activated chain end. Therefore, in a homogeneous ATRP, where the distance between chain ends is large, such mass transport effects are negligible. In the confined ATRP experiments considered in this study, however, this distance is on the order of nanometers, and the effect is evidently substantial.

Conversely, the activation of a dormant chain would locally enrich the environment with $Cu^{II}X_2$ while depleting $Cu^{I}X$ (Figure 9b). Because at equilibrium, the rate of activation and deactivation must balance, it is important to consider why these enrichment/depletion events do not cancel each other. The probability of finding the $Cu^{II}X_2$ formed in an activation event again scales as $t^{-3/2}e^{-r^2/t}$, and thus it should encounter other chain ends in the local vicinity. However, because these other chain ends are likely to be dormant, this local excess of $Cu^{II}X_2$ should have no effect. Additionally, the replenishment of the locally depleted $Cu^{I}X$ will be a significantly faster process because of its higher bulk concentration relative to $Cu^{II}X_2$. Moreover, the diffusivity of $Cu^{I}X$ should be greater than that of $Cu^{II}X_2$ owing to its comparatively smaller size. Therefore, collectively, the surface-initiated system experiences a net local elevation in $[Cu^{I}X]$ at the expense of $[Cu^{II}X_2]$ because of mass transport effects induced by the elevated local viscosity and small chain-end-to-chain-end distances.

Similar arguments suggest that the local monomer concentration in the "viscous front" may be depleted in the neighborhood of an active chain, owing to the reduced monomer diffusivity and elevated local viscosity. This depletion should again scale with the local chain concentration and, in principle, should oppose the acceleration due to the shift in the local catalyst concentration. In our experiments, however, we do not observe monomer exclusion effects because the monomer plays a dual role as solvent. Therefore, any depletion event induces a strong concentration gradient such that the time scale for monomer diffusion to the active site is still much shorter than that of the propagation reaction. Accordingly, we suspect that local monomer depletion effects may become observable in dilute monomer/solvent systems.

In consideration of these enrichment/depletion arguments, we may construct a simple phenomenological model that encapsulates the effects of this coupled network of mass transport and reaction events. In the "viscous front", chain ends locally experience net catalyst concentrations of $[Cu^{I}X] = \langle[Cu^{I}X]\rangle + \delta$ and $[Cu^{II}X_2] = \langle[Cu^{II}X_2]\rangle - \delta$, where $\langle ... \rangle$ denotes the homogeneous equilibrium concentration. The local deviation, δ, should be proportional to the local chain concentration, $\propto (\sigma\rho_{g,max})^{3/2}$, and will be influenced by a host of factors including the activation/deactivation rate constants and the local diffusivity. We introduce a dimensionless lumped "effectiveness"

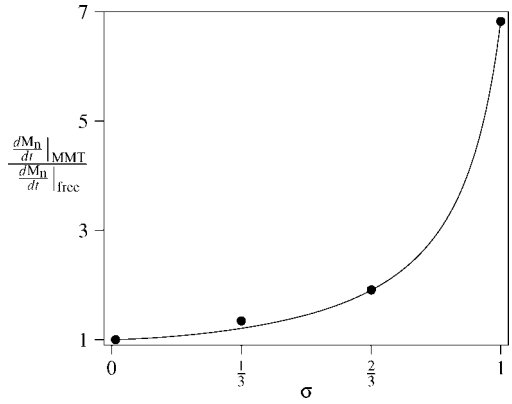

Figure 10. Propagation rates, relative to bulk ATRP of PS, of PS-*graft*-MMT produced by SI-ATRP. The data are fit with a single parameter, λ, using the relationship of eq 5. For a 16.7:1 molar ratio of CuBr/CuBr$_2$, $\lambda = 0.864$.

parameter, λ, that incorporates these considerations such that $\delta = \lambda(\sigma\rho_{g,max})^{3/2}$. Accordingly, the acceleration of dM_n/dt relative to an ATRP from free initiators may be expressed as

$$\frac{\frac{dM_n}{dt}\text{MMT}}{\frac{dM_n}{dt}\text{free}} = \frac{\langle[Cu^{II}X_2]\rangle}{\langle[Cu^{I}X]\rangle}\frac{\langle[Cu^{I}X]\rangle + \lambda(\sigma\rho_{g,max})^{\frac{3}{2}}}{\langle[Cu^{II}X_2]\rangle - \lambda(\sigma\rho_{g,max})^{\frac{3}{2}}} \quad (5)$$

Free initiator kinetics are recovered as $\sigma \rightarrow 0$. As shown in Figure 10, this single-parameter model reproduces our kinetic data with $\lambda = 0.864$.

Our results support the plausibility of this simple enrichment/delpletion model and demonstrate that the kinetics of surface-initiated ATRP under certain conditions, that is, in the strong brush regime, depart significantly from an analogous ATRP from free initiators. These considerations become important in the context of molecular design. Moreover, caution should be exercised in experiments in which both tethered and free initiators are employed, because inferences of the molecular weight distribution of the brush layer derived from that of the free polymer may be flawed.

5. Summary

The kinetics of polystyrene brush polymerization from MMT clay by SI-ATRP was investigated as a function of graft density and compared with bulk ATRP of styrene under analogous conditions. A seven-fold increase in PS growth rate was observed, relative to bulk kinetics, at the highest graft density, ~1 chain/nm^2. Bulk kinetics were rapidly recovered as the graft density was reduced. We hypothesized that local concentration heterogeneities shift the ATRP equilibrium in favor of the active state and developed a single-parameter kinetic model based on this hypothesis that was able to account for our kinetic data. These findings present an important consideration relevant to the design of precisely defined molecular architectures from surfaces using surface-initiated ATRP.

Acknowledgment. E.W.C. is grateful for support from the Camille and Henry Dreyfus New Faculty Award Program and the Petroleum Research Fund, award no. 48399-G7.

References and Notes

(1) Matyjaszewski, K.; Xia, J. Atom transfer radical polymerization. *Chem. Rev.* **2001**, *101*, 2921–2990.
(2) Xia, J.; Matyjaszewski, K. Controlled/"living" radical polymerization. *Macromolecules* **1997**, *30*, 7697–7700.
(3) Xia, J.; Zhang, X.; Matyjaszewski, K. The Effect of Ligands on Copper-Mediated Atom Transfer Radical Polymerization. In *Transition Metal Catalysis in Macromolecular Design*; Boffa, L. S., Novak, B. M., Eds.; ACS Symposium Series 760; American Chemical Society: Washington, D.C., 2000; pp 207−223.
(4) Ohno, K.; Morinaga, T.; Koh, K.; Tsujii, Y.; Fukuda, T. Synthesis of monodisperse silica particles coated with well-defined, high-density polymer brushes by surface-initiated atom transfer radical polymerization. *Macromolecules* **2005**, *38*, 2137–2142.
(5) Boettcher, H.; Hallensleben, M. L.; Nuss, S.; Wurm, H.; Bauer, J.; Behrens, P. Organic/inorganic hybrids by "living"/controlled ATRP grafting from layered silicates. *J. Mater. Chem.* **2002**, *12*, 1351–1354.
(6) Kim, J.-B.; Huang, W.; Miller, M. D.; Baker, G. L.; Bruening, M. L. Kinetics of surface-initiated atom transfer radical polymerization. *J. Polym. Sci., Part A: Polym. Chem.* **2003**, *41*, 386–394.
(7) Kaholek, M.; Lee, W.-K.; Ahn, S.-J.; Ma, H.; Caster, K. C.; LaMattina, B.; Zauscher, S. Stimulus-responsive poly(*n*-isopropylacrylamide) brushes and nanopatterns prepared by surface-initiated polymerization. *Chem. Mater.* **2004**, *16*, 3688–3696.
(8) Jones, D. M.; Brown, A. A.; Huck, W. T. S. Surface-initiated polymerizations in aqueous media: Effect of initiator density. *Langmuir* **2002**, *18*, 1265–1269.
(9) Xiao, D.; Wirth, M. J. Kinetics of surface-initiated atom transfer radical polymerization of acrylamide on silica. *Macromolecules* **2002**, *35*, 2919–2925.
(10) Wu, T.; Efimenko, K.; Vlcek, P.; Subr, V.; Genzer, J. Formation and properties of anchored polymers with a gradual variation of grafting densities on flat substrates. *Macromolecules* **2003**, *36*, 2448–2453.
(11) Tomlinson, M. R.; Efimenko, K.; Genzer, J. Study of kinetics and macroinitiator efficiency in surface-initiated atom-transfer radical polymerization. *Macromolecules* **2006**, *39*, 9049–9056.
(12) Brittain, W. J., Boyes, S. G., Granville, A. M.; Baum, M., Mirous, B. K., Akgun, B., Zhao, B., Blickle, C.; Foster, M. D. Surface Rearrangement of Diblock Copolymer Brushes-Stimuli Responsive Films. In *Surface-Initiated Polymerization II*; Jordan, R., Ed.; Advances in Polymer Science Series 198; Springer: Berlin, 2006; pp 125−147.
(13) Uhlmann, P.; Ionov, L.; Houbenov, N.; Nitschke, M.; Grundke, K.; Motornov, M.; Minko, S.; Stamm, M. Surface functionalization by smart coatings: stimuli-responsive binary polymer brushes. *Prog. Org. Coat.* **2006**, *55*, 168–174.
(14) Yang, Y.; Liu, L.; Zhang, J.; Li, C.; Zhao, H. Pmma colloid particles stabilized by layered silicate with pmma-*b*-pdmaema block copolymer brushes. *Langmuir* **2007**, *23*, 2867–2873.
(15) Giannelis, E. P., Krishnamoorti, R.; Manias, E. Polymer−Silicate Nanocomposites: Model Systems for Confined Polymers and Polymer Brushes. In *Polymers in Confined Environments*; Binder, K., Ed.; Advances in Polymer Science Series 138; Springer: Berlin, 1999; pp 107−147.
(16) Weimer, M. W.; Chen, H.; Giannelis, E. P.; Sogah, D. Y. Direct synthesis of dispersed nanocomposites by in situ living free radical polymerization using a silicate-anchored initiator. *J. Am. Chem. Soc.* **1999**, *121*, 1615–1616.
(17) Pyun, J.; Matyjaszewski, K. Synthesis of nanocomposite organic/inorganic hybrid materials using controlled/"living" radical polymerization. *Chem. Mater.* **2001**, *13*, 3436–3448.
(18) Yamamoto, S.; Ejaz, M.; Tsujii, Y.; Fukuda, T. Surface interaction forces of well-defined, high-density polymer brushes studied by atomic force microscopy. 2. Effect of graft density. *Macromolecules* **2000**, *33*, 5608–5612.
(19) Jeyaprakash, J. D.; Samuel, S.; Dhamodharan, R.; Ruhe, J. Polymer brushes via ATRP: role of activator and deactivator in the surface-initiated atrp of styrene on planar substrates. *Macromol. Rapid Commun.* **2002**, *23*, 277–281.
(20) Matyjaszewski, K.; Miller, P.; Shukla, N.; Immaraporn, B.; Gelman, A.; Luokala, B.; Siclovan, T.; Kickelbick, G.; Vallant, T.; Hoffmann, H.; Pakula, T. Polymers at interfaces: Using atom transfer radical polymerization in the controlled growth of homopolymers and block copolymers from silicon surfaces in the absence of untethered sacrificial initiator. *Macromolecules* **1999**, *32*, 8716–8724.
(21) Shen, Y.-H. Estimation of surface area of montmorillonite by ethylene oxide chain adsorption. *Chemosphere* **2002**, *48*, 1075–1079.
(22) Zhao, H.; Farrell, B. P.; Shipp, D. A. Nanopatterns of poly(styrene-*block*-butyl acrylate) block copolymer brushes on the surfaces of exfoliated and intercalated clay layers. *Polymer* **2004**, *45*, 4473–4481.
(23) Keller, R. N.; Wycoff, H. D. 1. Copper(I) Chloride. *Inorg. Synth.* **1946**, *2*, 1–4.
(24) LeBaron, P. C.; Wang, Z.; Pinnavaia, T. J. Polymer-layered silicate nanocomposites: an overview. *Appl. Clay Sci.* **1999**, *15*, 11–29.
(25) Matyjaszewski, K.; Patten, T. E.; Xia, J. Controlled/"living" radical polymerization. kinetics of the homogeneous atom transfer radical polymerization of styrene. *J. Am. Chem. Soc.* **1997**, *119*, 674–680.

MA8024909